Comparison between the machinability of different titanium alloys (Ti-6Al-4V and Ti-6Al-7Nb) employing the multi-objective optimization

Amanda Oliveira Mello[1], Robson Bruno Dutra Pereira[1], Carlos Henrique Lauro[1,2], Lincoln Cardoso Brandão[1], J. Paulo Davim[2]

[1] Federal University of São João del-Rei, Department of Mechanical Engineering, Centre for Innovation in Sustainable Manufacturing, Praça Frei Orlando, 170, Centro, 36.307-352, São João del Rei – Brazil

[2] University of Aveiro, Department of Mechanical Engineering, Campus Santiago, 3810-193 Aveiro, Portugal

amandamello@live.com; robsondutra@ufsj.edu.br; carlos.lauro@ua.pt; lincoln@ufsj.edu.br

Abstract: *Titanium and its alloys are amongst the most important metallic materials used by many industries, such as those pertaining to the aerospace, automotive, and biomedical sectors. This is due to the reliability and functionality of titanium components, in addition to their high strength-to-weight ratio and corrosion resistance. Thus, titanium and its alloys are of great importance to the challenging operations of these sectors. The manufacturing of titanium requires great accuracy to ensure that resulting products meet quality requirements, due to its difficult machinability. In this study, the cutting forces and surface roughness of the turning were analysed to compare different titanium alloys, Ti-6Al-4V and Ti-6Al-7Nb, with CVD-coated and uncoated inserts. The effect of control factors on the response variables was measured using ANOVA. Response surface methodology was applied to the creation of a model of responses and to a bi-objective optimization process via the normalized normal constraint method. The Pareto-optimal sets of both alloys were achieved, which may be applied to practical situations to achieve optimal results for these responses. The models and optimization results confirmed the similarity of machinability values between the Ti-6Al-4V and Ti-6Al-7Nb alloys. The uncoated inserts yielded the best surface roughness and cutting force results when used with both titanium alloys.*

Keywords: *Titanium alloys; Cutting force; Surface roughness; Multi-objective optimization.*

1. Introduction

Over the last years, improvements in materials and manufacturing processes have promoted the perception of titanium and its alloys as some of the main metallic materials used in several industries, especially in the biomedical sector. Their high strength-to-weight ratio, corrosion resistance and great endurance in high-temperature environments are very useful to the aerospace industry [1]. According to Hashmi *et al*. [2], titanium alloys are used due to the reliability and functionality of parts created

using them and are thus of great importance to the challenging operations of these sectors. However, titanium alloys are commonly known as difficult-to-cut materials [3] because of the high temperature generated during their machining process, which increases tool wear rates and reduces surface finish quality [4].

Different chemical compositions of titanium alloys are available to meet the demands of important industrial sectors. The Ti-6Al-4V alloy is the most commonly used titanium alloy, and it is employed in the production of aerospace and biomedical components. It is composed of 6% aluminium, which stabilizes the α phase, and 4% vanadium, which stabilizes the β phase [2]. Its integration of biomedical components, however, has been widely criticized due to the presence of vanadium, which is a potentially toxic metal.

Still, according to Gallego *et al*. [5], an alloy with similar properties, containing niobium instead of vanadium as stabilizing element of the β phase, was developed. Niobium has excellent biocompatibility and, when associated with aluminium, accounts for most of the solid strengthening of the alloy [6]. Moreover, the microstructure of both alloys consists of a α-Ti phase and a β-Ti phase, which are a good compromise and justify their employment in several biomechanical applications.

Still, in order to use titanium alloys correctly, especially as biomedical components, a previously setup of the manufacturing cell is necessary. Machine tools, tooling settings, cutting conditions and cooling systems are the main factors responsible for keeping product quality during machining processes. Furthermore, the optimization of machining processes represents a bottleneck to production lines, not only due to the high-level manufacturing requirements of these components, but also because of the high price of raw materials. These factors require minimal losses in waste, which in machining is generally formed by chips.

Surface roughness is the main response variable used to measure the surface quality of the machined surface of a workpiece. According to Dietzsch *et al*. [7], there are many different surface roughness profiles in use nowadays in modern industry, with R_a being by far the most commonly applied in shop-floor activities. In terms of tribology, surfaces with high R_a values generally wear more quickly and have lower corrosion resistance and higher friction coefficients than surfaces with lower R_a values.

Several investigations have analysed the role of surface roughness as a reference and main response of turning processes [8]. Khan *et al*. [9] obtained R_a values of 0.51 to 3.91 μm during turning processes. Moreover, when the feed rate was 0.14 mm/rev, surface roughness was less than 0.80 μm, regardless of the tool condition. These authors tested chamfered tools and demonstrated that this kind of tool not only outperformed conventional tool geometries, but also yielded results similar to those obtained using polycrystalline diamond-coated tooling under the same conditions.

Sun *et al*. [10] used polycrystalline cubic boron nitride (PCBN) and polycrystalline diamond (PCD) cutting tools in the dry machining of Ti-6Al-4V alloys. The authors demonstrated that surface roughness increased gradually, but after the feed rate of 0.1 mm/rev, there was a reduction of the adhered workpiece material and the thermal softening of the alloy. This situation provided a special condition to the machining process studied by the authors, where surface roughness maintained a constant value.

Ribeiro Filho *et al*. [11] demonstrated that the R_a and R_z surface roughness parameters were influenced mainly by the feed rate, which accounted for 98.98% and 96.55% of *Ra* and *Rz*, respectively. The authors analysed the surface roughness parameters of Ti-6Al-4V alloys to find the best range for the input parameters of their machining process and to define the desired corrosion performance of their machined surfaces in a simulated body fluid environment. Considering the surface roughness of biomedical components, the difference between rough or smooth surface values can result in good or poor osseointegration in the human body, which depends on specific applications.

In the machining of titanium alloys, diffusion is the main wear mechanism, since it is worsened by the high temperature generated during the cutting process. Therefore, oil-based flood coolants have been used to dissipate the temperature of the cutting region. However, the oil in them causes several environmental damages and increases machining costs [12]. Several researchers have proposed dry turning as a feasible alternative to achieve a more sustainable production chain of titanium alloy components [4, 9, 12].

To achieve the cutting conditions necessary to guarantee low roughness levels, optimization should be applied. The optimization of manufacturing processes can vary according to the response chosen to be improved, via e.g. cost reduction, production time reduction, reduction of cutting forces, improvement of surface roughness, reduction of tool wear, or improvement of special aspects for biomedical components. The optimization process may also combine two or more of these objectives; in this case, it is called multi-objective optimization. In the literature can be found several studies that employed the multi-objective optimization in different machining processes, like turning [13], milling [14], electrical discharge machining [15], abrasive water jet [16], and other processes.

Several industrial problems are multi-objective involving the optimization of distinct criteria simultaneously. In these cases, the researcher does not look for a single optimal solution, but a set of non-dominated solutions, also known as a Pareto-optimal set [17, 18]. Several popular multi-objective techniques are based on scalarization. Some multi-objective scalarization approaches, such as Normalized Normal Constraint (NNC), convert the multi-objective problem into a single objective problem, setting one function as objective and allocating the remaining ones in the constraints [19].

Response surface methodology (RSM) was developed as a statistical and mathematical collection of tools for modelling and optimization. RSM has been used to study several manufacturing processes. To optimize surface roughness when turning Ti-6Al-4V alloys at high speeds, Hashmi *et al*. [2] employed a model based on RSM. According to the authors, in practical situations where a specific surface roughness value is specified, machine operators can use the proposed model to set the optimum values of machining parameters. However, it is known that statistical models are conservative regarding tool, machine, fixture and other conditions used in tests.

Mia *et al*. [20] obtained statistical models through RSM that are recommended for predicting surface roughness and cutting forces in the turning of Ti-6Al-4V alloys. These models had very promising coefficient of determination values above 96%, which indicated the optimum results to be: R_a surface roughness of 1.05 μm, feed force of 208 N, and cutting force of 315 N. Furthermore, according to the results obtained by the authors, with regard to analyses of cutting forces and surface roughness, RSM was more accurate when using untrained data, in comparison to artificial neural network models.

Sangwan *et al*. [21] used artificial neural networks and genetic algorithms to predict the surface roughness in Ti-6Al-4V machining. According to the authors, feed rate was the main input parameter, but considering depth of cut and cutting speed, surface roughness was at its lowest value only when these input parameters were increased. However, the authors concluded that more studies need to be carried out using a wide range of machining parameters to generalize these results.

Satyanarayana *et al*. [22] employed the Grey-Taguchi method to optimize the Ti-6Al-4V machining process. The authors defined that the order of importance of controllable factors to achieve minimum surface roughness is, from the most important to the least important factor, rake angle, feed rate, depth of cut, and cutting speed. Other studies were performed modelling the surface roughness resulting from the turning of Ti-6Al-4V alloys [23, 24].

The preliminary studies demonstrated important results obtained by the machining of Ti-6Al-4V alloys. This work analyses the optimization of the turning process of two main titanium alloys, Ti-6Al-4V and Ti-6Al-7Nb. Precision manufacturing of titanium alloy is indispensable to ensure that the quality requirements of products – such as biomedical components – are met, and thus to obtain a great surface quality that is essential to improve corrosion resistance. The optimization of this process also provides a social benefit due to its reduction of cutting forces, which saves energy and/or tools. To achieve these goals, RSM was used for the creation of models, and the normalized normal constraint multi-objective optimization method was applied.

2. Experimental procedure and methods

A CNC lathe from Romi, GL 240M model, with maximum spindle speed of 6,000 rpm and power of 22.5 kW was used to carry out the cutting tests. The workpieces were made of Ti-6Al-4V and Ti-6Al-7Nb alloys with approximately 32 HR_C. The cutting tests were performed using two different inserts, TCMT 110304-H13A (uncoated) and TCMW 110304-3215 (CVD-coated - TICN+AL2O3+TIN), on a STGCL 1616H 11-B1 holder. Both inserts and the holder were configured using the same cutting parameters: cutting speed (v_c), depth of cut (a_p), and feed rate (f) based on catalogue of the tool manufacturer. The workpiece was set up with an overhang length of 15 mm without tailstock to avoid the influence of vibrations on surface roughness, with a cutting length of 14 mm for each test. The cutting parameter values were fixed in accordance with the tool manufacturer catalogue. The turning tests were carried out under dry condition. Figure 1 shows the experimental setup for studying the turning of different titanium alloys.

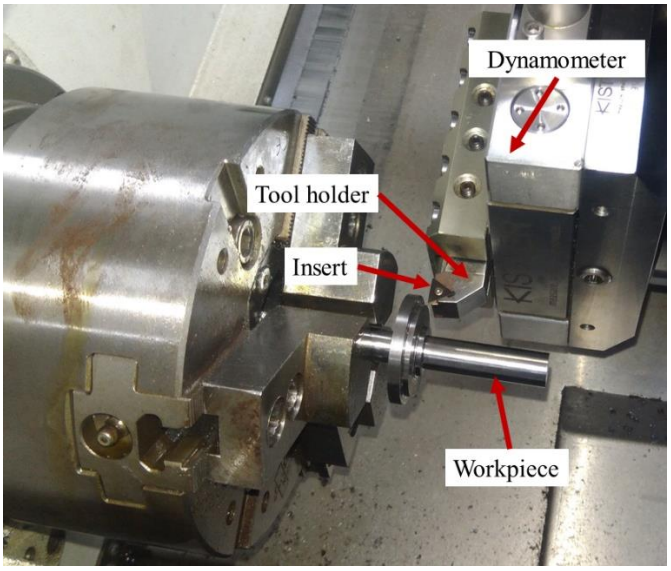

Figure 1 - Experimental setup

2.1. Treatment of Responses

A Kistler 9129AB30 piezoelectric dynamometer was used to monitor cutting forces, using an acquisition rate of 500 Hz to observe the components of the machining force (F_M), cutting force (F_c), feed force (F_f), and passive force (F_p). The signal processing method employed was based on Lauro *et al*. [25], applying the wavelet transform to denoise the signal. The mathematical model for the F_M force, Eq. 1, takes into account the F_c, F_f, and F_p forces, point-to-point, of each experimental test and defines the influence of input parameters on F_M. A SJ-401 Mitutoyo surftest was used to measure

surface roughness. The R_a surface roughness was measured with a cut-off of 0.8 mm near the middle of the cutting length in three radially equidistant points of 120° for each test.

$$F_{M_{av}} = \frac{\sum_0^i \sqrt{F_{c_i}^2 + F_{f_i}^2 + F_{p_i}^2}}{n} \quad (1)$$

Where F_{Mav} is the machining force average [N]; F_c is the cutting force [N]; F_f is the feed force [N]; F_p is the passive force [N]; i is the time increment; and n is the number of increments.

2.2. Statistical analysis, modelling and multi-objective optimization

The significance of the continuous and categorical factors to the two responses, R_a and F_M, was tested using Analysis of variance (ANOVA). However, for both R_a and F_M, response surface models were created considering each insert type in each titanium alloy. For all statistical tests, the significance level was $\alpha = 0.05$.

Response surface methodology (RSM) is a conventional statistical tool to formulate an approximate mathematical relationship, mainly for optimization, of dependent variables – such as F_M force, and R_a surface roughness – based on independent variables, such as cutting speed (v_c), feed rate (f), depth of cut (a_p), and insert type. The use of a second-order approximate function in the form of Eq. 2 is useful to understand the effects of the control variables on the response and, especially, to achieve the optimal levels of the parameters in the response. The study of surface roughness combined with cutting forces in the turning process has been performed previously using statistical and optimization tools [26].

$$\hat{y} = \beta_0 + \sum_{i=1}^{k} \beta_i x_i + \sum_{i=1}^{k} \beta_{ii} x_i^2 + \sum \sum_{i<j} \beta_{ij} x_i x_j \quad (2)$$

In the response model represented by Eq. 2, y is the dependent variable; β_0 is the constant term; β_i, β_{ii}, β_{ij} are the coefficients of linear, quadratic, and cross product terms, respectively; and x_i, i = 1, …, k, are the input or control variables. To achieve a response surface in the form of Eq. 2, the experimental planning used was a central composite design (CCD) with k = 3 continuous factors. The same design was applied to design the turning tests of both Ti-6Al-4V and Ti-6Al-7Nb. Considering the three continuous variables – v_c, f and a_p –, $n_F = 2^3 = 8$ factorial points, $n_C = 6$ centre points, and $n_A = 2 \times 3 = 6$ axial points were performed for each one of the 2 inserts. Therefore, the CCD accounted for 40 turning tests for each titanium alloy. Table 1 shows the parameter levels of the experimental tests.

Table 1 - Input parameters used in experimental tests.

Input parameters	Levels				
	-1.63	-1	0	1	+1.63
v_c [m/min]	50	55.07	62.50	69.93	75
f [mm/rev]	0.05	0.09	0.15	0.21	0.25
a_p [mm]	0.20	0.36	0.60	0.84	1.00
Insert	TCMT 110304-H13A			TCMW 110304-3215	

A multi-objective optimization task with m multi-objective functions may be defined as follows, with $f_i(\boldsymbol{x})$ as the i-th objective function, $i = 1, \ldots, m$, and $\boldsymbol{x} = [x_1, \ldots, x_K]^T$ as the design vector, subject to the inequality constraints, $\boldsymbol{g}(\boldsymbol{x}) \geq \boldsymbol{0}$, the equality constraints, $\boldsymbol{h}(\boldsymbol{x}) = \boldsymbol{0}$, and limited to the lower and upper bounds, $\boldsymbol{L}$ and $\boldsymbol{U}$.

$$
\begin{aligned}
&Min\ \boldsymbol{f}(\boldsymbol{x}) = [f_1(\boldsymbol{x}) \quad \cdots \quad f_i(\boldsymbol{x}) \quad \cdots \quad f_m(\boldsymbol{x})]^T \\
&\text{Subject to:} \quad \boldsymbol{g}(\boldsymbol{x}) \geq \boldsymbol{0} \\
&\qquad\qquad\ \ \boldsymbol{h}(\boldsymbol{x}) = \boldsymbol{0} \\
&\qquad\qquad\ \ \boldsymbol{L} \leq \boldsymbol{x} \leq \boldsymbol{U}
\end{aligned}
\tag{3}
$$

An important concept in multi-objective optimization, is to evaluate the trade-off between the objective functions, is the pay-off matrix. A general pay-off matrix $\boldsymbol{\Phi}$ is exposed as follows. Each individual minimum is denoted as $f_i^*(\boldsymbol{x}_i^*)$, $i = 1, \ldots, m$, and stored in the main diagonal. The columns of the pay-off matrix are the anchor points, i.e., $\boldsymbol{f}_i^* = [f_1(\boldsymbol{x}_i^*) \quad \cdots \quad f_i^*(\boldsymbol{x}_i^*) \quad \cdots \quad f_m(\boldsymbol{x}_i^*)]^T$, $i = 1, \ldots, m$. In each row of the pay-off matrix, it is possible to identify the individual minima and aggregate these values defining a utopia vector as $\boldsymbol{f}^U = [f_1^*(\boldsymbol{x}_1^*) \quad \cdots \quad f_i^*(\boldsymbol{x}_i^*) \quad \cdots \quad f_m^*(\boldsymbol{x}_m^*)\ ]^T$. In the same way, it is also possible to define a vector of worst results for each function, taking the worst result of each row, and aggregating them in the commonly called pseudo-nadir vector, $\boldsymbol{f}^{PN} = [f_1^{PN} \quad \cdots \quad f_i^{PN} \quad \cdots \quad f_m^{PN}]^T$, with $f_i^{PN} = Max\,\{f_i(\boldsymbol{x}_1^*) \quad \cdots \quad f_i^*(\boldsymbol{x}_i^*) \quad \cdots \quad f_i(\boldsymbol{x}_m^*)\}$, $i = 1, \ldots, m$. The nadir point is obtained through the maximization of each objective function subject to the constraints of the problem.

$$
\boldsymbol{\Phi} = \begin{bmatrix}
f_1^*(\boldsymbol{x}_1^*) & \cdots & f_1(\boldsymbol{x}_i^*) & \cdots & f_1(\boldsymbol{x}_m^*) \\
\vdots & \ddots & \vdots & \ddots & \vdots \\
f_i(\boldsymbol{x}_1^*) & \cdots & f_i^*(\boldsymbol{x}_i^*) & \cdots & f_i(\boldsymbol{x}_m^*) \\
\vdots & \ddots & \vdots & \ddots & \vdots \\
f_m(\boldsymbol{x}_1^*) & \cdots & f_m(\boldsymbol{x}_i^*) & \cdots & f_m^*(\boldsymbol{x}_m^*)
\end{bmatrix}
\tag{4}
$$

To avoid scale and unit effects, the multi-objective optimization should be performed in the normalized space. The *i*-th normalized objective function denoted according to the Eq. 5, where $\bar{\boldsymbol{\Phi}}$ is the normalized pay-off matrix and $\bar{\boldsymbol{f}}_i^*$ are the normalized anchor points, $i = 1, \ldots, m$. The normalized utopia and pseudo-nadir vectors are denoted as $\bar{\boldsymbol{f}}^U = [0 \quad \cdots \quad 0 \quad \cdots \quad 0]^T$ and $\bar{\boldsymbol{f}}^{PN} = [1 \quad \cdots \quad 1 \quad \cdots \quad 1]^T$, respectively. Therefore, in the normalized solution space, $\bar{f}_i \in [0,1]$, $i = 1, \ldots, m$.

$$\bar{f}_i = \frac{f_i - f_i^*}{f_i^{PN} - f_i^*} \tag{5}$$

The simultaneous optimization of multiple objectives results in a set of optimal solutions rather than a single optimal solution [27]. Therefore, after the response surface models were obtained, bi-objective optimization for R_a and F_M was performed using the Normalized Normal Constraint (NNC) method [28]. Kosaraju and Anne [29] carried out a similar investigation on Ti-6Al-4V turning. The authors used the desirability approach, setting the desired weight for each outcome and calculating an agglomerating metric, to obtain only one optimal solution to the responses. The present study proposes the application of a multi-objective method to achieve a set of Pareto solutions in the turning of titanium alloys, allowing a trade evaluation of R_a and F_M and providing the experimenter the possibility of choosing the most appropriate solution for each scheduling situation.

The sequential quadratic programming method was used to achieve Pareto-optimal solutions, which are stochastic solutions, with goodness-of-fit measure values determining its predictability in relation to the response surface models. Some multi-objective optimization tasks suggest the application of mathematical criteria agglomerating all the responses to achieve a general optimal solution through the optimization of the selected criteria [30]. In some cases, it can be useful for experimenters to formulate distinct scenarios, thus allowing the choice of a solution for each planning requirement. This possibility is only possible using procedures that will return a set of solutions within the set of trade-off choices among the responses commonly called Pareto frontier. The NNC is an interesting method of accomplishing this, since it allows a good filling of the Pareto frontier.

For the bi-objective case the NNC method can be formulated as shown in Eq. 6, with $\bar{f}_1$ and $\bar{f}_2$ as the normalized objective functions of interest; and w_{1j} and w_{2j}, $j = 1, \ldots, n_{sub}$, as the weights associated with $\bar{f}_1$ and $\bar{f}_2$, where n_{sub} is the desired number of Pareto optimal solutions. The w_{1j} and w_{2j} weights should respect $w_1 + w_2 = 1$ and $0 << w_1, w_2 << 1$. To achieve a set of solutions that are well distributed throughout the Pareto frontier, w_1 and w_2 should be varied considering a constant spacing,

i.e. $\delta = 1/m_1 - 1$. This study employed n_{sub} = 51 and, consequently, δ = 0.02. For more details about NNC formulation and procedures, see [31].

$$Min\ \bar{f}_2 \tag{6}$$
$$Subject\ to:$$
$$\bar{f}_1 - \bar{f}_2 + w_{1j} - w_{2j} \leq 0$$

The NNC method is formulated through the Eq. 7. $\bar{f}_m(\boldsymbol{x})$ is the *m*-th objective function; $\bar{\boldsymbol{n}}_r$ are the utopia line vectors, calculated as $\bar{\boldsymbol{n}}_r = \bar{f}_m^* - \bar{f}_r^*$, r = 1, …, m – 1; $\bar{\boldsymbol{f}}$ is the vector of objective functions under optimization; and $\boldsymbol{q}_{j,m\times 1}$, j = 1, …, n_{sub} are the points in the utopia plane. These points are defined considering the weights w_{ij} as $\boldsymbol{q}_{j,m\times 1} = \sum_{i=1}^{m} w_{ij} \times \bar{\boldsymbol{f}}_i^*$, with $\sum_{i=1}^{m} w_{ij} = 1$ and $0 \leq w_{ij} \leq 1$, i = 1, …, m. These points are indexed with j = 1, …, n_{sub}, where n_{sub} is the number of sub-problems to be solved to achieve the desired Pareto set. The utopia plane is the triangular region defined through the anchor points. The product between the utopia line vector $\bar{\boldsymbol{n}}_r^T$ and the vector $\left(\bar{\boldsymbol{f}} - \boldsymbol{q}\right)$ are set to be less or equal to zero, resulting in a quasi-orthogonality between these two vectors. Through this inequality, a constrained optimal solution $\bar{\boldsymbol{f}}$ is achieved in the Pareto frontier. The procedure is repeated into a loop considering the weights, w_{ij}, variation which will change $\boldsymbol{q}$, j = 1, …, n_{sub}.

$$Min\ \bar{f}_m(\boldsymbol{x})$$
$$\text{Subject to: } \bar{\boldsymbol{n}}_r^T\left(\bar{\boldsymbol{f}} - \boldsymbol{q}\right) \leq 0,\ r = 1, \ldots, m-1$$
$$\boldsymbol{g}(\boldsymbol{x}) \geq \boldsymbol{0}$$
$$\boldsymbol{h}(\boldsymbol{x}) = \boldsymbol{0}$$
$$\boldsymbol{L} \leq \boldsymbol{x} \leq \boldsymbol{U} \tag{7}$$

To achieve the desired number of solutions n_{sub}, it is required to define the spacing between weights, δ_r, and the number of subproblems, n_{sub}, to be solved. The number of subproblems is calculated according to Eq. 8, where $\eta_r = 1 + 1/\delta_r$. For, instance, for m = 2 objective functions, the NNC method can be solved considering Algorithm 1.

$$n_{sub} = \binom{m + \eta_r - 2}{\eta_r - 1} \tag{8}$$

3. Analysis of the results

As the same design was used for both titanium alloys, initially a *t*-paired test was performed to gauge the differences in the R_a surface roughness and F_M force resulting from the turning of Ti-6Al-4V and Ti-6Al-7Nb alloys. To apply the *t*-paired test, the assumption of normality of these differences must be confirmed. To acquire the difference in R_a between both alloys, the Anderson-Darling (*AD*) normality test resulted in a *p*-value < 0.005, rejecting the null hypothesis of normality. Consequently, instead of the parametric *t*-paired test, the non-parametric sign test was applied to the R_a differences obtained, resulting in a *p*-value = 0.1996, concluding that the hypothesis of the difference equal to zero should not be rejected. For F_M, the normality test to determine its differences resulted in a *p*-value = 0.652, guaranteeing that there is no evidence to reject the null hypothesis of normality of the differences. Then, the *t*-paired test was performed, resulting in a *p*-value = 0.861. Consequently, the null hypothesis of the difference in F_M between the two alloys was not rejected. Therefore, the results of R_a surface roughness and F_M force differences amongst both alloys were similar in general.

Table 2 shows the ANOVA of R_a and F_M with respect to both alloys. The effects of the control factors on the Ti-6Al-4V alloy can be observed in Figure 2, and Figure 3**Erro! Fonte de referência não encontrada.** shows the effects of F_M and R_a on Ti-6Al-7Nb. Regarding F_M, only the cutting speed (v_c) did not produce a statistically significant linear effect on it. The linear effect of both significant factors – feed rate (f) and depth of cut (a_p) – on F_M was positive, and the Uncoated inserts demonstrated a lower average, as confirmed in Figure 2a. Safari *et al*. [32] observed plastic deformation on the surface of the coated carbide tool. In addition, surface roughness for uncoated inserts did not improve when the cutting speed increased and the uncoated inserts provided surface roughness, mainly at lower cutting speed, than the coated inserts. The linear effects were similar in relation to both alloys. Regarding the square effects, the square feed rate was statistically significant only in the turning of Ti-6Al-7Nb, with a downward, almost imperceptible convexity, as illustrated in Figure 3a. In the analysis of interactions, only the a_p*f interaction was statistically significant for the F_M of both alloys. Analysing Figure 2a and Figure 3a, it can be noted that, when the depth of cut is raised, the effect of the feed rate on F_M grows proportionally. This is due to the increase in the cross-section area of the uncut chip.

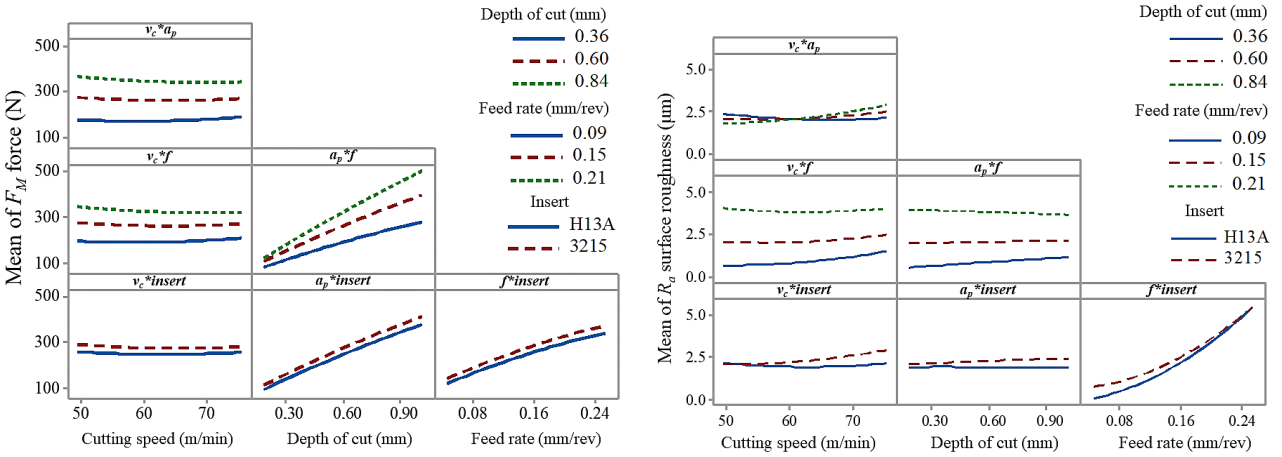

a) F_M force b) R_a surface roughness

Figure 2 - Interaction plot of the Ti-6Al-4V alloy

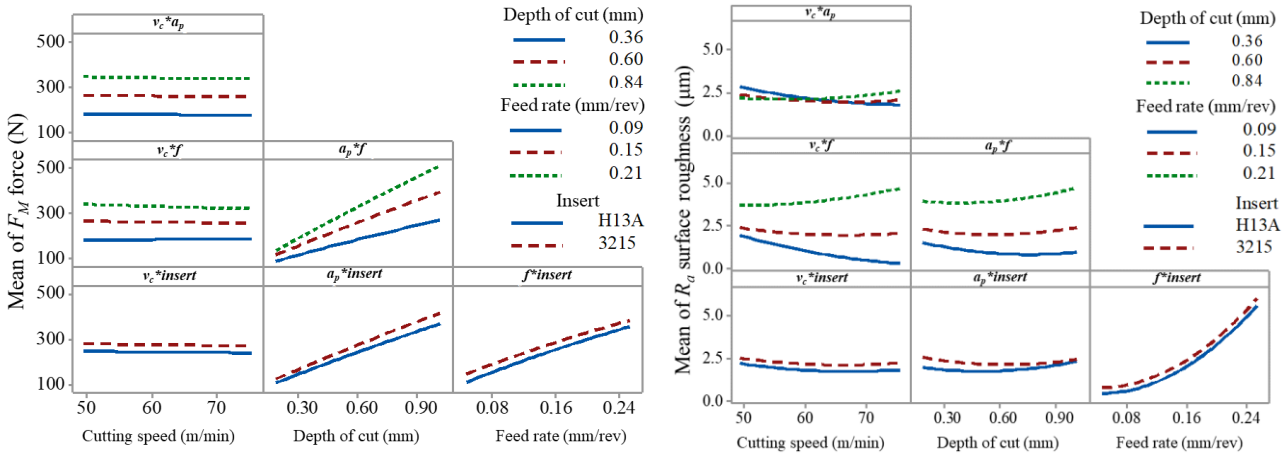

a) F_M force b) R_a surface roughness

Figure 3 - Interaction plot of the Ti-6Al-7Nb alloy

Table 2 - Analysis of variance of surface roughness (R_a) and machining force (F_M)

Source	Ti-6Al-4V				Ti-6Al-7Nb			
	F_M		R_a		F_M		R_a	
	F-value	P-Value	F-value	P-Value	F-value	P-Value	F-value	P-Value
v_c	0.24	0.626	2.06	0.163	0.53	0.471	0.65	0.426
a_p	650.21	*0.000*	0.27	0.605	648.13	*0.000*	0.08	0.783
f	389.86	*0.000*	313.36	*0.000*	501.55	*0.000*	172.48	*0.000*
insert	25.09	*0.000*	6.88	*0.014*	38.00	*0.000*	3.68	0.066
v_c * v_c	1.28	0.269	0.83	0.371	0.01	0.917	0.51	0.480
a_p * a_p	1.17	0.290	0.01	0.926	0.36	0.555	1.21	0.281
f * f	2.64	0.116	11.61	*0.002*	1.35	*0.000*	13.56	*0.001*
v_c * a_p	1.41	0.246	3.37	0.078	0.02	0.885	2.03	0.166
v_c * f	1.74	0.199	1.24	0.276	0.78	0.385	6.62	*0.016*
v_c * *insert*	0.11	0.743	2.39	0.134	0.00	0.950	0.01	0.913
a_p * f	38.88	*0.000*	1.53	0.228	47.23	*0.000*	1.69	0.205

a_p * *insert*	0.42	0.525	0.50	0.487	1.85	0.185	0.38	0.541
f * *insert*	0.17	0.682	1.34	0.258	0.12	0.733	0.00	0.945
Lack-of-Fit	2.78	0.053	2.43	0.078	1.47	0.271	0.78	0.684
For factors test: $F_{(\alpha=0.05;df1=1;df2=26)}$=4.225; For lack-of-fit test: $F_{(\alpha=0.05;df1=16;df2=10)}$=2.828;								
Normality test								
AD (p-value)	0.312	(0.537)	0.395	(0.356)	0.647	(0.085)	0.636	(0.091)
Goodness of fit								
S	17.36 N		0.43 µm		16.60 N		0.60 µm	
R^2_{adj}	0.9658		0.8949		0.9692		0.829	
R^2_{pred}	0.9293		0.7937		0.9453		0.7158	

On the other hand, the input parameters that showed a linear effect with statistical significance, p-value < α = 0.05, on R_a were *f*, for both alloys, with positive effect, and the tool, for the Ti-6Al-4V alloy, with the Uncoated insert having lower R_a than 3215, as confirmed in Figure 2b. The feed rate generally produces a significant effect on the surface roughness of parts obtained by turning, due to the periodic geometric feature of the tool left on the generated surface. Only the square feed rate (f) was significant to both alloys. Observing Figure 2b and Figure 3b, the curvature had upward convexity. As to the interactions, the $v_c \times f$ interaction was statistically significant to the R_a of the Ti-6Al-7Nb alloy. With the increase of the cutting speed, the effect of the feed rate on surface roughness was higher; furthermore, with lower feed rate, the cutting speed had a negative effect on R_a. Conversely, when the feed rate was higher, cutting speed had a positive effect on R_a during the turning of Ti-6Al-7Nb, as observed in Figure 3b.

As summarized in Table 2, lack-of-fit tests were performed to analyse all responses, and they found no evidence to reject the null hypothesis of no lack of fit. The *AD* normality test was also carried out to analyse all responses, guaranteeing no evidence to reject the hypothesis of normality of the residuals. As to the goodness-of-fit statistics, considering R^2_{adj}, all models demonstrated at least 92% experimental data variability, and, with regard to R^2_{pred}, all models showed at least 79% predictability, except for the R_a response of the Ti-6Al-7Nb alloy, which had 71.58%.

The experiments acquired a surface roughness range of 0.24 to 5.61 µm when using the Ti-6Al-4V alloy, while with the Ti-6Al-7Nb alloy the surface roughness results of the experiments were in the range of 0.42 to 6.09 µm. The best surface roughness value found during the experimental tests was 0.24 µm, and this value is close to that of the parts finished using grinding. According to Mello *et al*. [33], the range of R_a values in the patterns of titanium workpieces was 0.5 to 0.9 µm. Thus, the dry turning of titanium alloy parts with a quality approximate to that of grinding processes can be achieved, as was obtained in the present study.

Carou *et al*. [34] carried out experimental turning tests using Ti-6Al-4V alloys, and found surface roughness values of 0.7 µm for a feed rate of 0.1 mm/rev. The authors highlight that the influence of

the feed rate was noticeable, as well as that of cutting speed. High feed rate levels generated high surface roughness values. High surface roughness values represent not only poor surface quality – which can increase the friction between parts –, but also poor corrosion resistance. According to Ribeiro Filho *et al*. [11], the passivation rate of Ti-6Al-4V alloys is related to minimum surface errors attained using low surface roughness. Surface roughness can define the workpiece quality and is very important to the determination of its corrosion behaviour, which is of great importance when manufacturing biomedical components.

Despite the higher R_a following the increasing of the feed rate, the use of different tools also influenced surface roughness, as can be seen in Figure 2b and Figure 3b. The TCMW 110304-H13A inserts yielded better surface roughness values than the TCMT 110304-3215 inserts. Thus, comparing the geometries of both, it should be taken into consideration that the CVD-coated inserts does not have a uncoated inserts, unlike the uncoated inserts, which has one, and consequently has a positive secondary rake angle. Based on this, it can be stated that the use of uncoated inserts can provide better surface roughness due to the shear mechanism allowed by the chip-curling mode, with restricted contact length, which reduces friction, temperature, and forces, as confirmed experimentally by this study.

Mia *et al*. [20] demonstrated that the use of tools with positive rake angle provides a free chip flow during Ti-6Al-4V turning. According to the results obtained by authors, regardless of the feed rate used in the turning, the three feed values showed the same behaviour.

With regard to machining force, its range was of 101.69 N to 422.23 N and 98.88 N to 478.29 N for the Ti-6Al-4V and Ti-6Al-7Nb alloys, respectively. The depth of cut and feed rate are the main responsible factors for the directly proportional variation of the cutting force in the cutting cross-section during turning, as well as for the product of the feed rate and depth of cut, as seen in Table 2, Figure 2a and Figure 3a. Thus, with a constant specific cutting pressure, the increase of only feed rate and depth of cut or both of them creates a proportional increase in cutting force. Since the depth of cut is of a greater order of magnitude, its linear effect on F_M was prominent. Furthermore, the f^*a_p interaction, which is statistically significant to both alloys, demonstrates this relation, since the linear effect of depth of cut grows proportionally to the increase of feed rate.

The use of high feed rate and depth of cut values can reduce production time, but it will also increase tool wear, and plastic deformation of the tool can occur. Therefore, extreme turning conditions may guarantee a reduction of cutting time, but they may also cause the acceleration of tool wear mechanisms. Considering the effect of the inserts type on F_M, the uncoated insert had better results than the CVD-coated insert with regard to both Ti-6Al-4V and Ti-6Al-7Nb due to the influence of the

rake angle on chip formation and temperature generated during the turning process, as previously explained.

The study carried out by Khan *et al*. [9] showed the same behaviour in the turning of a Ti-6Al-4V alloy. According to the authors, lower levels of feed rate were responsible for lower cutting forces and temperature, but, on the other hand, higher levels of feed rate accounted for a lower chip reduction coefficient. However, optimal levels of cutting parameters (feed rate, cutting speed, and depth of cut) need to be achieved to ensure the desired level of the response chosen.

By performing the statistical analysis, it can be noted that the two titanium alloys behaved similarly during the turning tests, and the Uncoated inserts had the best results for both responses. Therefore, the response surface models for the R_a and *FM* of both titanium alloys with the use of the Uncoated inserts have been chosen for optimization.

In Figure 4 and Figure 5 are shown the response surface plots for the F_M and R_a of Ti-6Al-4V and Ti-6Al-7Nb turning processes, respectively. Table 3 summarizes the uncoded response surface models of responses using both inserts and alloys. All models had good data variability account, with $R^2_{adj} \geq 79\%$, and good predictability, with $R^2_{\text{pred}} \geq 72\%$.

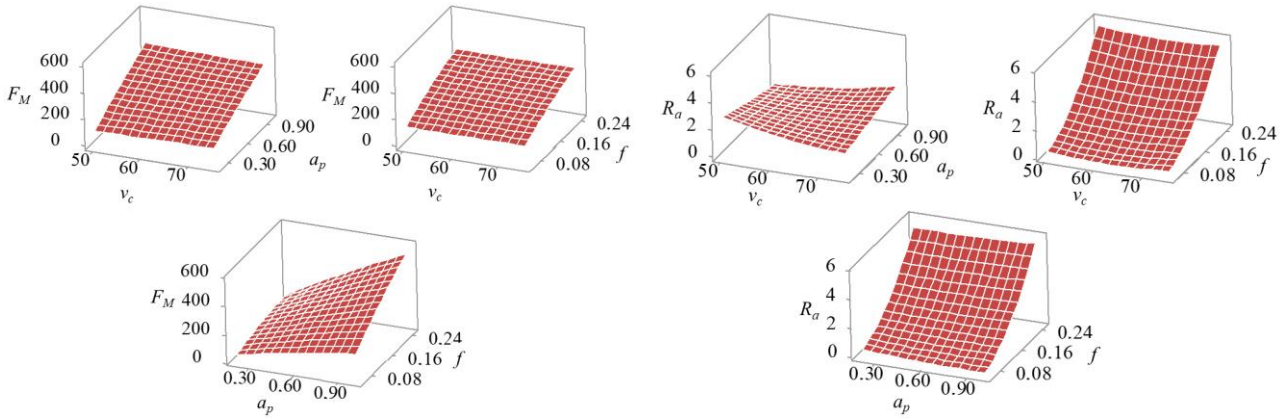

a) F_M force b) R_a surface roughness

Hold values: cutting speed of 62.5 m/min; depth of cut of 0.6 mm; feed rate of 0.15 mm/rev

Figure 4 - Response surfaces of Ti-6Al-4V alloy and uncoated inserts

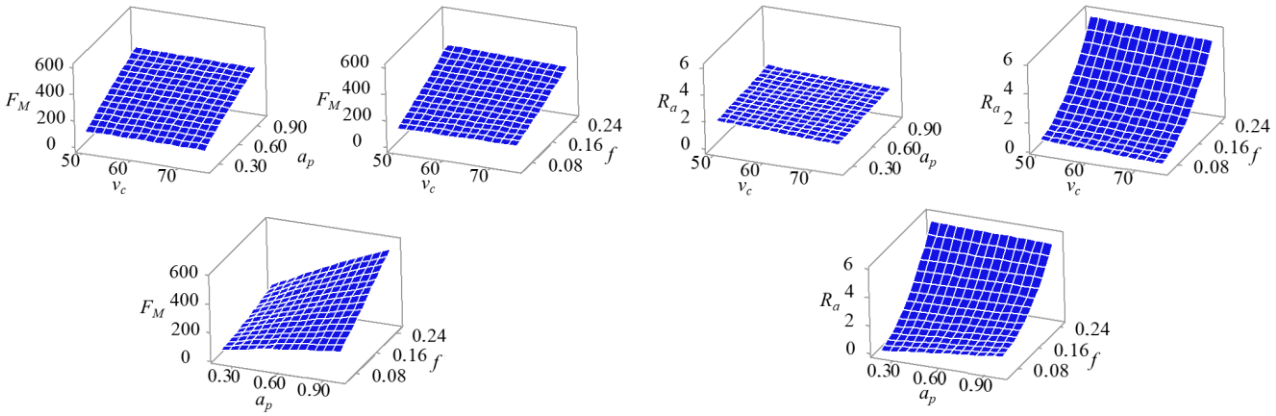

a) F_M force b) R_a surface roughness

Hold values: cutting speed of 62.5 m/min; depth of cut of 0.6 mm; feed rate of 0.15 mm/rev

Figure 5 - Response surfaces of Ti-6Al-7Nb alloy and uncoated inserts

Table 3 - Uncoded response surface models

	Ti-6Al-4V	Goodness of fit
H13A	$Ra = 10.76 - 0.251 \times vc - 9.02 \times ap - 3.3 \times f + 0.00141 \times vc^2 + 0.50 \times a_p{}^2 + 93.8 \times f^2 + 0.1265 \times vc \times ap - 0.013 \times vc \times f + 3.03 \times ap \times f$	R^2_{adj} = 94.69%; R^2_{pred} = 79.05%
	$Ft = -36 - 0.37 \times vc + 255.2 \times ap + 569 \times f + 0.0091 \times vc^2 - 65 \times ap^2 - 1736 \times f^2 - 1.41 \times vc \times ap + 0.07 \times vc \times f + 1682 \times ap \times f$	R^2_{adj} = 99.39%; R^2_{pred} = 98.40%
3215	$Ra = -0.9 - 0.095 \times vc - 0.88 \times ap + 48.6 \times f + 0.00121 \times vc^2 - 0.76 \times ap^2 + 59.2 \times f^2 + 0.085 \times vc \times ap - 0.500 \times vc \times f - 20.9 \times ap \times f$	R^2_{adj} = 82.26%; R^2_{pred} = 44.58%
	$Ft = 131 - 9.4 \times vc + 393 \times ap + 1840 \times f + 0.121 \times vc^2 - 57 \times ap^2 - 1193 \times f^2 - 4.08 \times vc \times ap - 24.5 \times vc \times f + 1926 \times ap \times f$	R^2_{adj} = 93.30%; R^2_{pred} = 72.80%
	Ti-6Al-7Nb	**Goodness-of-fit**
H13A	$Ra = 1.25 - 0.0140 \times vc + 0.428 \times ap - 7.2 \times f + 107.0 \times f^2$	R^2_{adj} = 86.80%; R^2_{pred} = 77.08%
	$Ft = -146 + 3.97 \times vc + 200 \times ap + 390 \times f - 0.0217 \times vc^2 - 77.1 \times ap^2 - 999 \times f^2 - 0.62 \times vc \times ap - 7.8 \times vc \times f + 1652 \times ap \times f$	R^2_{adj} = 97.44%; R^2_{pred} = 92.21%
3215	$Ra = 28.7 - 0.501 \times vc - 15.73 \times ap - 102.8 \times f + 0.00200 \times vc^2 + 2.87 \times ap^2 + 120.7 \times f^2 + 0.114 \times vc \times ap + 1.149 \times vc \times f - 33.2 \times ap \times f$	R^2_{adj} = 79.90%; R^2_{pred} = 74.08%
	$Ft = 102 - 3.3 \times vc + 16 \times ap + 1257 \times f + 0.0333 \times vc^2 + 12.8 \times ap^2 - 3000 \times f^2 - 0.02 \times vc \times ap - 7.8 \times vc \times f + 2151 \times ap \times f$	R^2_{adj} = 96.90%; R^2_{pred} = 91.40%

The Pareto frontier of R_a and F_M is shown in Figure 6. Regarding the Ti-6Al-4v alloy, the best result of R_a under multi-objective optimization was R_a^* = 0.46 μm, with the adjustments to the levels of control variables to minimize R_a, as represented by $\mathbf{x}_{[Ra^*]}$ = [v_c = 66.4 m/min, a_p = 0.48 mm, f = 0.06 mm/rev]^T. By applying $\mathbf{x}_{[Ra^*]}$ to F_M, F_M = 114.5 N was obtained. In contrast, the optimal F_M value, 92.8 N, was acquired using control factor levels $\mathbf{x}_{[Ft^*]}$ = [v_c = 62 m/min, a_p = 0.24 mm, f = 0.11 mm/rev]^T. When these optimal levels of control factors are applied to R_a, R_a = 0.94 μm is obtained. Consequently,

the Pareto frontier explores different scenarios under these limits called anchor points, which define the trade-off limits between R_a and F_M.

For Ti-6Al-7Nb, the best R_a result was $R_a^* = 0.46$ µm, when using the levels of control variables that minimize R_a: $\mathbf{x}_{[Ra^*]} = [v_c = 66.4$ m/min, $a_p = 0.48$, $f = 0.06$ mm/rev$]^T$. By applying $\mathbf{x}_{[Ra^*]}$ to F_M, $F_M = 121.35$ N was acquired. A minimization of F_M, $F_M^* = 91.05$ N, was reached using $\mathbf{x}_{[FM^*]} = [v_c = 62$ m/min, $a_p = 0.23$ mm, $f = 0.11$ mm/rev$]^T$. When applying these optimal levels to R_a, $R_a = 1.02$ µm is obtained. As can be noted, the turning of both alloys resulted in similar optimal levels of control factors.

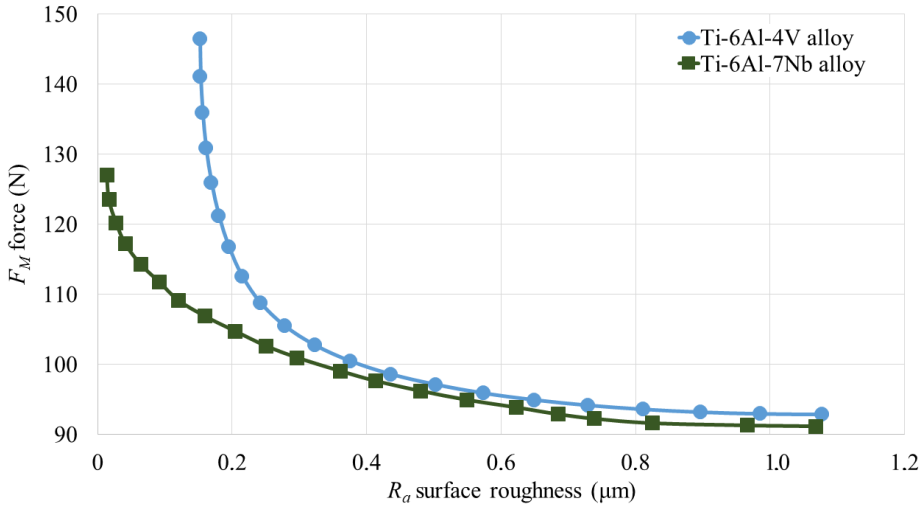

Figure 6 - Pareto frontier of R_a surface roughness and F_M force using the uncoated inserts

The Pareto frontiers in Figure 6 contain some possibilities for planning the turning process of titanium alloys. Each Pareto optimal solution has distinct R_a and F_M values and related optimal levels of design variables. There is no dominated Pareto solution in both fronts, which gives the experimenter the reliability of selecting the most interesting solutions to each planning situation. To better explore these solutions, Table 4 demonstrates 11 of the 51 solutions plotted for each titanium alloy, with w_1 as the weight that defines the R_a preference, $1 - w_1$ as the weight associated with F_M, and all the Pareto-optimal levels of R_a and F_M.

Table 4 - Pareto optimal solutions for R_a and F_M, Ti-6Al-4V and Ti-6Al-7Nb, Uncoated inserts

w_1	Ti-6Al-4V					Ti-6Al-7Nb				
	Control factors' levels			Pareto solutions		Control factors' levels			Pareto solutions	
	v_c	a_p	f	R_a	F_M	v_c	a_p	f	R_a	F_M
	m/min	mm	mm/rev	µm	N	m/min	mm	mm/rev	µm	N
0	62	0.24	0.11	0.94	92.8	62	0.23	0.11	1.02	91.1

0.1	62	0.25	0.10	0.85	93.0	62	0.24	0.11	0.91	91.3
0.2	62	0.26	0.10	0.76	93.4	62	0.25	0.10	0.81	92.1
0.3	62	0.28	0.09	0.68	94.1	62	0.27	0.09	0.73	93.5
0.4	62	0.31	0.08	0.61	95.3	63	0.29	0.09	0.65	95.5
0.5	63	0.34	0.07	0.55	97.0	63	0.31	0.08	0.59	98.0
0.6	63	0.37	0.07	0.51	99.4	63	0.34	0.07	0.54	101.3
0.7	64	0.41	0.06	0.48	102.5	64	0.38	0.07	0.50	105.3
0.8	65	0.43	0.06	0.47	106.2	65	0.41	0.06	0.47	110.1
0.9	66	0.46	0.06	0.46	110.3	66	0.44	0.06	0.46	115.5
1	66	0.48	0.06	0.46	114.5	66	0.48	0.06	0.46	121.4

The distance between the Pareto-optimal solutions and the experimental solutions are shown in Figure 7. As can be observed in Figure 7a, with regard to Ti-6Al-4V, there is no experimental solution with better results than the Pareto-optimal solutions obtained through the NNC multi-objective optimization method. However, there is an experimental result, with R_a = 0.38 μm and F_M = 132.3 N, that is not dominated by the Pareto solutions. implying that this solution may be comparable to such Pareto solutions, since it has little roughness, albeit with the trade-off of losing turning force. Since the optimized models of R_a and F_M force are approximations, the Pareto solutions have confidence limits. When comparing the experimental values with the Pareto-optimal solutions, it is clear that the Pareto frontier brings better results with regard to these two variables that should be minimized.

Regarding Ti-6Al-7Nb, in Figure 7b, it is notable that an experimental point dominates some Pareto-optimal solutions, i.e. the result with R_a = 0.42 μm and F_M = 115.8 N. This can also be explained due to the statistical fluctuation expected for each solution, with respect to the R_a and F_M models. However, the difference between this experimental result and the Pareto solutions is negligible. In general, the Pareto optimal solutions offered boundary possibilities to achieve optimal response results. In practice, the engineer may select the appropriate solution in Table 4 to each scheduling situation, to achieve desired R_a and F_M levels by programming the associated levels of v_c, a_p and f. For both titanium alloys, the experimental results demonstrated a larger amplitude than the Pareto solutions. The Pareto solutions compose boundaries to explore the trade-off between roughness and turning force in the turning of titanium alloys.

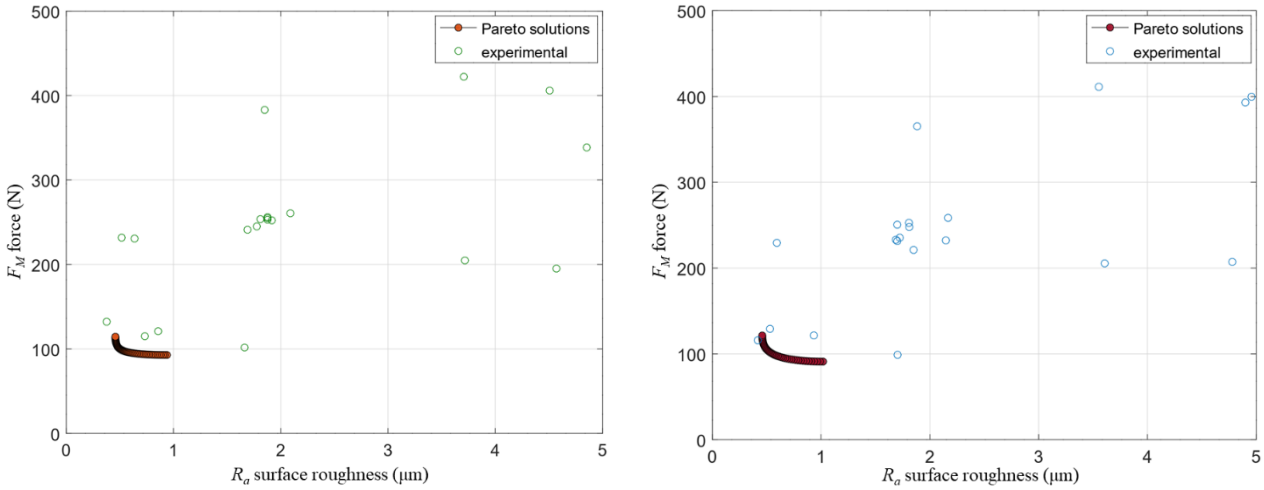

a) Ti-6Al-4V alloy b) Ti-6Al-7Nb alloy

Figure 7 - Pareto frontier with experimental results for the uncoated inserts

Figure 8 shows the overlaid contour plot for R_a and $F_{M,}$ with the correspondent design space values for each Pareto frontier when using the Ti-6Al-7Nb alloy. All contour plots were obtained with v_c fixed in its individual optima, since v_c was generally the cutting parameter that had the lowest effect on the responses, and in the Pareto-optimal solutions the variation in v_c was inferior in percentage when compared to the variation in f and a_p, as presumed through Table 4. Consequently, it can be observed in Figure 8 that, in the case of both alloys, the possible levels of a_p and f provide interesting R_a and F_M scenarios. It can also be noted, in the legend of the following figures, that the Pareto solutions in the design space denoted by "*" for Ti-6Al-4V (Figure 8a) and by "+" for Ti-6Al-7Nb (Figure 8b) are delimitated by the experimental constraint, which is a sphere since the central composite design was employed as the statistical experimental planning paradigm. Therefore, despite the fact that results with lower R_a and F_M can be found inside the frontier observed in the design space, these solutions are not feasible, since the regression models of both responses keep their prediction properties only in the experimental region.

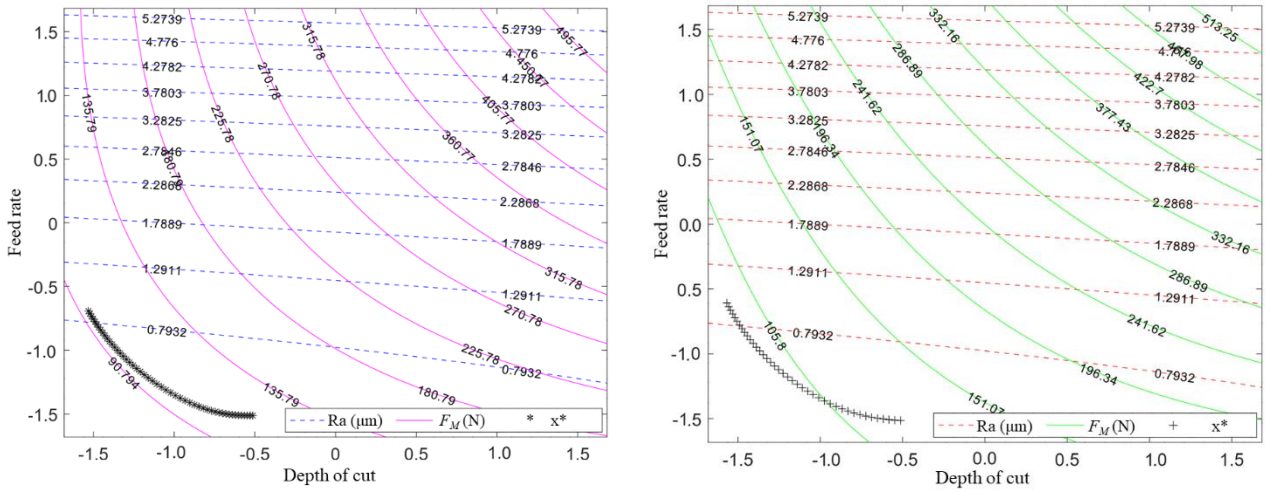

a) Ti-6Al-4V alloy b) Ti-6Al-7Nb alloy

Figure 8 - Overlaid contour plot of R_a and F_M

As illustrated in Figure 7 and Figure 8, the turning processes Ti-6Al-V and Ti-6Al-7Nb had similar experimental results, models and Pareto-optimal results. Therefore, it can be concluded that both alloys have similar machinability during the turning process. The models and optimal results obtained may be useful as a reference for engineers and other workers dealing with the dry turning of these important materials in several industrial sectors, such as the automotive and medical industries. For a conclusive visualization, Figure 9 is presented to corroborate the machinability correspondence of both alloys. The percentage of contribution of the most important effects to F_t is shown in Figure 10(a), with a_p followed by f as the most important effects to both titanium alloys. Figure 10(b) shows the most important effects to *Ra*, which were f – responsible for a large part of the contribution –, followed by the quadratic effect f^2, in the case of both titanium alloys.

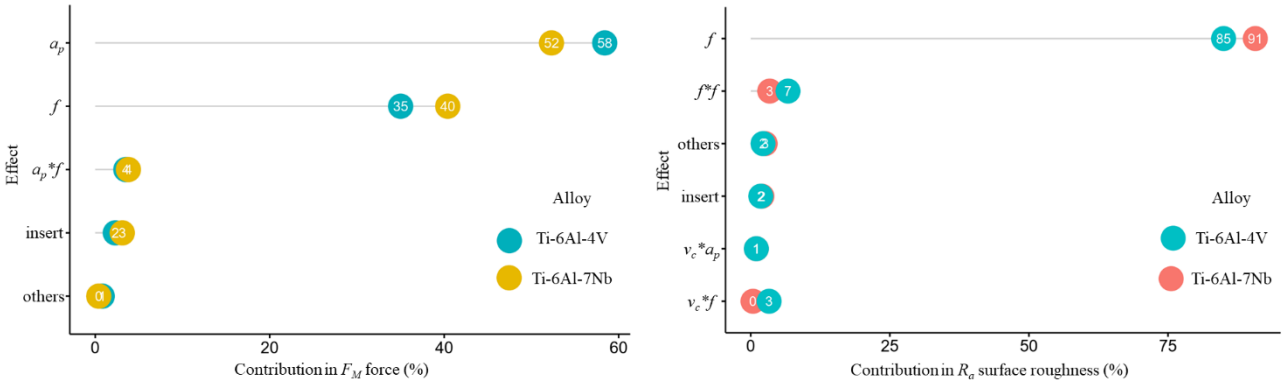

a) F_M force b) R_a surface roughness

Figure 9 - Contribution of effects to Ti-6Al-4V and Ti-6Al-7Nb turning

4. Conclusions

This study assessed the turning processes of two important titanium alloys under dry condition. Cutting forces and surface roughness were investigated in experimental tests, and the results were discussed. They can be summarized as follows:

✓ The experimental range of values of R_a surface roughness for the Ti-6Al-4V alloy was lower than Ti-6Al-7Nb alloy. However, the range of F_M force for Ti-6Al-4V alloy was higher than Ti-6Al-7Nb alloy. Statistically supported, uncoated insert had lower R_a and F_M because it was used uncoated insets, ensuring a low contact area on the rake face, in addition to low cutting forces and roughness.

✓ The statistical significance of the Analysis of Variance (ANOVA) method was supported by a good fit. Considering the control factors, with regard to both alloys, a_p and f were statistically significant to F_M, with a positive effect, while only f was significant to R_a, also with a positive effect. The quadratic effects were statistically significant only to f in the case of both the R_a and F_M of Ti-6Al-7Nb.

✓ Response surface models were obtained for each insert in each titanium alloy. For both R_a and F_M responses, the models demonstrated a good fit and can be employed to predict practical values of R_a and F_M when varying turning conditions.

✓ For the Ti-6Al-4V inserts, the multi-objective optimization through the Normalized Normal Constraint (NNC) method located the anchor point for R_a surface roughness with optimal control factors levels: $\mathbf{x}_{[Ra^*]} = [v_c = 66.4$ m/min, $a_p = 0.48$ mm, $f = 0.06$ mm/rev$]^T$, with $R_a^* = 0.46$ μm and $F_M = 114.5$ N. In the other extreme, the anchor point of F_M force was obtained: $\mathbf{x}_{[FM^*]} = [v_c = 62$ m/min, $a_p = 0.24$ mm, $f = 0.11$ mm/rev$]^T$, with $F_M^* = 92.8$ N and μm $R_a = 0.94$ μm. Intermediate results were achieved, populating the Pareto frontier, allowing the experimenter to define the preferred results for each outcome by using weights.

✓ The multi-objective optimization of the Ti-6Al-7Nb alloy acquired the following anchor point for R_a: $\mathbf{x}_{[Ra^*]} = [v_c = 66.4$ m/min, $a_p = 0.48$, $f = 0.06$ mm/rev$]^T$, $R_a^* = 0.46$ μm and $F_M = 121.35$ N. With respect to the turning force, the anchor point was: $\mathbf{x}_{[FM^*]} = [v_c = 62$ m/min, $a_p = 0.23$ mm, $f = 0.11$ mm/rev$]^T$, with $F_M^* = 91.05$ N and $R_a = 1.02$ μm. The Pareto frontier stores options to attain intermediate scenarios considering this trade-off. For both titanium alloys the results in terms of R_a, F_M and control factor levels' v_c, a_p and f were very similar, ensuring similar machinability of both Ti-6Al-4V and Ti-6Al-7Nb.

Acknowledgments

The authors would like to thank the CNPq - Brazilian National Research Council for its financial support through the productivity research scholarship granted. Additional thanks go to the TiFast S.r.l.

Funding

This work is also supported by FAPEMIG - Minas Gerais Research Foundation for its financial support to Project APQ-01987/14 and Foundation for Science and Technology (FCT), Portugal (Project no. 031556-FCT/02/SAICT/2017; FAMASI - Sustainable and Intelligent Manufacturing by Machining, financed by FCT/POCI)

References

1. Raza SW, Pervaiz S, Deiab I (2014) Tool wear patterns when turning of titanium alloy using sustainable lubrication strategies. Int J Precis Eng Manuf 15:1979–1985. https://doi.org/10.1007/s12541-014-0554-z
2. Hashmi KH, Zakria G, Raza MB, Khalil S (2016) Optimization of process parameters for high speed machining of Ti-6Al-4V using response surface methodology. Int J Adv Manuf Technol 85:1847–1856. https://doi.org/10.1007/s00170-015-8057-3
3. Li N, Kong YCD (2019) Multi-response optimization of Ti-6Al-4V turning operations using Taguchi-based grey relational analysis coupled with kernel principal component analysis. Adv Manuf. https://doi.org/10.1007/s40436-019-00251-8
4. Maroju NK, Pasam VK (2019) FE Modeling and Experimental Analysis of Residual Stresses in Vibration Assisted Turning of Ti6Al4V. Int J Precis Eng Manuf 20:417–425. https://doi.org/10.1007/s12541-019-00021-3
5. Gallego J, Pinheiro TS, Valiev RZ, et al (2012) Microstructural characterization of Ti-6Al-7Nb alloy after severe plastic deformation. Mater Res 15:786–791. https://doi.org/10.1590/S1516-14392012005000100
6. Khan MA, Williams RL, Williams DF (2002) The corrosion behaviour of Ti–6Al–4V, Ti–6Al–7Nb and Ti–13Nb–13Zr in protein solutions. Biomaterials 20:631–637. https://doi.org/10.1016/s0142-9612(98)00217-8
7. Dietzsch M, Papenfub K, Hartmann T (1998) The MOTIF-method (ISO 12085) — a suitable description for functional, manufactural and metrological requirements. Int J Mach Tools Manuf 38:625–632
8. Yadav RN (2017) Development and experimental investigation of duplex turning process. Adv Manuf 5:149–157. https://doi.org/10.1007/s40436-017-0177-6
9. Khan SA, Afzal MZ, Saleem MQ, et al (2018) Performance evaluation of novel chamfered

inserts in high-feed turning of Ti-6Al-4V alloy. Int J Adv Manuf Technol 97:2319–2329. https://doi.org/10.1007/s00170-018-2101-z

10. Sun FJ, Qu SG, Pan YX, et al (2015) Effects of cutting parameters on dry machining Ti-6Al-4V alloy with ultra-hard tools. Int J Adv Manuf Technol 79:351–360. https://doi.org/10.1007/s00170-014-6717-3
11. Ribeiro Filho SLM, Lauro CH, Bueno AHS, Brandão LC (2016) Influence cutting parameters on the surface quality and corrosion behavior of Ti–6Al–4V alloy in synthetic body environment (SBF) using Response Surface Method. Measurement 88:223–237. https://doi.org/10.1016/j.measurement.2016.03.047
12. You SH, Lee JH, Oh SH (2019) A Study on Cutting Characteristics in Turning Operations of Titanium Alloy used in Automobile. Int J Precis Eng Manuf 20:209–216. https://doi.org/10.1007/s12541-019-00027-x
13. Khan MA, Husain S, Jaffery I, et al (2020) Multi-objective optimization of turning titanium-based alloy Ti-6Al-4V under dry, wet, and cryogenic conditions using gray relational analysis (GRA). Int J Adv Manuf Technol 106:3897–3911. https://doi.org/10.1007/s00170-019-04913-6
14. Shihab SK, Gattmah J, Kadhim HM Experimental Investigation of Surface Integrity and Multi-Objective Optimization of End Milling for Hybrid Al7075 Matrix Composites. https://doi.org/10.1007/s12633-020-00530-1/Published
15. Ghodsiyeh D, Golshan A, Izman • S Multi-objective process optimization of wire electrical discharge machining based on response surface methodology. https://doi.org/10.1007/s40430-013-0079-x
16. A. Dumbhare P, Dubey S, V. Deshpande Y, et al (2018) Modelling and multi-objective optimization of surface roughness and kerf taper angle in abrasive water jet machining of steel. J Brazilian Soc Mech Sci Eng 40:1–13. https://doi.org/10.1007/s40430-018-1186-5
17. Zouache D, Ould Arby Y, Nouioua F, Ben Abdelaziz F (2019) Multi-objective chicken swarm optimization: A novel algorithm for solving multi-objective optimization problems. Comput Ind Eng 129:377–391. https://doi.org/10.1016/j.cie.2019.01.055
18. Vafaeenezhad T, Tavakkoli-Moghaddam R, Cheikhrouhou N (2019) Multi-objective mathematical modeling for sustainable supply chain management in the paper industry. Comput Ind Eng. https://doi.org/10.1016/J.CIE.2019.05.027
19. Emmerich MTM, Deutz AH (2018) A tutorial on multiobjective optimization : fundamentals and evolutionary methods. Nat Comput 17:585–609. https://doi.org/10.1007/s11047-018-9685-y

20. Mia M, Khan MA, Dhar NR (2017) Study of surface roughness and cutting forces using ANN, RSM, and ANOVA in turning of Ti-6Al-4V under cryogenic jets applied at flank and rake faces of coated WC tool. Int J Adv Manuf Technol 93:975–991. https://doi.org/10.1007/s00170-017-0566-9
21. Sangwan KS, Saxena S, Kant G (2015) Optimization of machining parameters to minimize surface roughness using integrated ANN-GA approach. Procedia CIRP 29:305–310. https://doi.org/10.1016/j.procir.2015.02.002
22. Satyanarayana K, Gopal AV, Babu PB (2014) Analysis for optimal decisions on turning Ti-6Al-4V with Taguchi-grey method. Proc Inst Mech Eng Part C J Mech Eng Sci 228:152–157. https://doi.org/10.1177/0954406213480599
23. Upadhyay V, Jain PK, Mehta NK (2013) In-process prediction of surface roughness in turning of Ti–6Al–4V alloy using cutting parameters and vibration signals. Measurement 46:154–160. https://doi.org/10.1016/j.measurement.2012.06.002
24. Karkalos NE, Galanis NI, Markopoulos AP (2016) Surface roughness prediction for the milling of Ti-6Al-4V ELI alloy with the use of statistical and soft computing techniques. Meas J Int Meas Confed 90:25–35. https://doi.org/10.1016/j.measurement.2016.04.039
25. Lauro CH, Ribeiro Filho SLM, Brandão LC, Davim JP (2016) Analysis of behaviour biocompatible titanium alloy (Ti-6Al-7Nb) in the micro-cutting. Measurement 93:529–540. https://doi.org/https://doi.org/10.1016/j.measurement.2016.07.059
26. Kalyon A, Günay M, Özyürek D (2018) Application of grey relational analysis based on Taguchi method for optimizing machining parameters in hard turning of high chrome cast iron. Adv Manuf 6:419–429. https://doi.org/10.1007/s40436-018-0231-z
27. Rao TB, Krishna AG, Katta RK, Krishna KR (2015) Modeling and multi-response optimization of machining performance while turning hardened steel with self-propelled rotary tool. Adv Manuf 3:84–95. https://doi.org/10.1007/s40436-014-0092-z
28. Messac A, Ismail-Yahaya A, Mattson CA (2003) The normalized normal constraint method for generating the Pareto frontier. Struct Multidiscip Optim 25:86–98. https://doi.org/10.1007/s00158-002-0276-1
29. Kosaraju S, Anne VG (2013) Optimal machining conditions for turning Ti-6Al-4V using response surface methodology. Adv Manuf 1:329–339. https://doi.org/10.1007/s40436-013-0047-9
30. Kumar R, Sahoo AK, Mishra PC, Das RK (2018) Comparative study on machinability improvement in hard turning using coated and uncoated carbide inserts: part II modeling, multi-response optimization, tool life, and economic aspects. Adv Manuf 6:155–175.

https://doi.org/10.1007/s40436-018-0214-0

31. Pereira RBD, da Silva LA, Lauro CH, et al (2019) Multi-objective robust design of helical milling hole quality on AISI H13 hardened steel by normalized normal constraint coupled with robust parameter design. Appl Soft Comput 75:652–685. https://doi.org/10.1016/J.ASOC.2018.11.040
32. Safari H, Sharif S, Izman S, et al (2014) Cutting Force and Surface Roughness Characterization in Cryogenic High-Speed End Milling of Ti–6Al-4V ELI. Mater Manuf Process 29:350–356. https://doi.org/10.1080/10426914.2013.872257
33. de Mello AV, de Silva RB, Machado ÁR, et al (2017) Surface Grinding of Ti-6Al-4V Alloy with SiC Abrasive Wheel at Various Cutting Conditions. Procedia Manuf 10:590–600. https://doi.org/10.1016/j.promfg.2017.07.057
34. Carou D, Rubio EM, de Agustina B, Teti R (2017) Sustainable Turning of the Ti-6Al-4V alloy at Low Feed Rates: Surface Quality Assessment. Procedia Manuf 8:769–774. https://doi.org/10.1016/j.promfg.2017.02.099